NANOSYSTEMS: PHYSICS, CHEMISTRY, MATHEMATICS, 2013, 4 (6), P. 851–856

FORMATION MECHANISM OF $GdFeO_3$ NANOPARTICLES UNDER THE HYDROTHERMAL CONDITIONS

E. A. Tugova[1,2], I. A. Zvereva[3]

[1]Ioffe Physical Technical Institute of RAS, Saint Petersburg, Russia

[2]Saint Petersburg Electrotechnical University "LETI", Saint Petersburg, Russia

[3]Saint Petersburg State University, Saint Petersburg, Russia

katugova@inbox.ru; irinazvereva@yandex.ru

PACS 61.46.+w

The formation mechanism of $GdFeO_3$ nanoparticles by varying of the hydrothermal conditions has been investigated. The mean size of coherent scattering regions of $GdFeO_3$ was determined to be equal to 53, 68 and 73 nm. The observed regularities allowed us to assume the oriented attachment of nanocrystals.

Keywords: nanoparticles, hydrothermal synthesis, nucleation, phase formation.

1. Introduction

Perovskite-type compounds possess unique electrical, magnetic, thermal properties [1-6]. The potential exists for materials production based on the application of perovskite-like oxide nanoparticles. However, in the literature there is little data concerning investigations into the chemical pre-history and synthetic technique's influence on size, morphology and properties of obtained $LnFeO_3$ (Ln = rare earth element) [7, 8]. The sonochemical method is suggested [9] for the synthesis of nanoparticles of the rare earth series of orthoferrites, using iron pentacarbonyl and rare earth carbonates as precursors. In this manner, $GdFeO_3$, $TbFeO_3$ nanoparticles of 60 nm and $EuFeO_3$, $ErFeO_3$ of 40 nm were obtained. According to the presented data [10] $LaFeO_3$ was synthesized by three different preparation methods, i.e., by the calcination of both mixtures of La_2O_3 and Fe_2O_3 (I), co-precipitated $La(OH)_3$ and $Fe(OH)_3$ hydroxides (II) and $La[Fe(CN)_6]\cdot 5H_2O$ heteronuclear complex (III). The formation of $LaFeO_3$ is recognized for I, II and III cases at calcining temperatures above 1000, 800 and 600 °C, respectively. The mean particle diameter of $LaFeO_3$ after heat treatment of $La[Fe(CN)_6]\cdot 5H_2O$ at 600 °C for 2 hours was 30 nm [10].

It was also shown [11, 12] that the mean size of coherent scattering regions, morphology and magnetic characteristics of $YFeO_3$ target product were strongly dependent upon the synthetic techniques. Besides, it is well known [13, 14], that hydrothermal synthesis allows the production of highly crystallized and well dispersed powders at relatively low temperatures. There is little literature concerning the hydrothermal synthesis of $LnFeO_3$ (Ln = rare earth element), particularly, $GdFeO_3$.

These reasons demonstrate the importance of systematic investigations of the peculiarities of nanocrystalline $GdFeO_3$ formation under hydrothermal conditions.

2. Experimental

2.1. Synthesis procedure

The initial mixture, corresponding to the stoichiometry of $GdFeO_3$ was prepared by precipitation method from aqueous solutions of stoichiometric amounts of 1M $Gd(NO_3)_3{\cdot}5H_2O$ and $Fe(NO_3)_3{\cdot}9H_2O$ by a previously published procedure [15]. The obtained powders were then transferred to autoclaves and heated at 300–480 ° C for 1–3 h under 60–90 MPa pressure in distilled aqueous media. The required pressure was determined by temperature and water filling content and produced on Kennedy table data [16]. After cooling, the product was unloaded and then dried at the ambient temperature.

2.2. Characterization of prepared nanocrystals

Purity and crystallization of $GdFeO_3$ samples were characterized by powder X-ray diffraction (XRD) using a Shimadzu XRD-7000 with monochromatic CuK_α radiation (λ= 154.178 pm). Crystallite sizes of the obtained powders were calculated by the X-ray line broadening technique based on Scherer's formula.

The microstructure of the specimen, elemental composition and the composition of separate phases were analyzed by means of scanning electron microscopy (SEM) using Quanta 200, coupled with EDAX microprobe analyzer. The error in determining the elements content by this method varies with the atomic number and equals to ±0.3 mass% on average.

3. Results and discussion

The performed X-Ray and SEM/EDAX analysis of co-precipitated initial mixture corresponding to the stoichiometry of $GdFeO_3$ shows the amorphous state and heterogeneity of the produced powders. But, it should be noted, that X-Ray diffraction pattern related to the initial mixture demonstrates the weak affect which can be attributed to hexagonal modification of $Gd(OH)_3$ (Fig. 1(1)).

TABLE 1. Electron probe microanalysis data for the regions indicated in Fig. 1($b-d$)

Sample	Sintering temperature ° C	Examined region	Components content, mol%		Phases
			$GdO_{1.5}$	$FeO_{1.5}$	
b	300	SQ1	36.58	63.42	$Gd_3Fe_5O_{12}$
		P1	38.67	61.33	$Gd_3Fe_5O_{12}$
		P2	17.92	82.08	Fe_2O_3
		P3	37.44	62.56	$Gd_3Fe_5O_{12}$
c	400	SQ2	43.97	56.03	$GdFeO_3$ + $Gd_3Fe_5O_{12}$
		P4	50.30	49.70	$GdFeO_3$
		P5	41.02	58.98	$GdFeO_3$ + $Gd_3Fe_5O_{12}$
		P6	46.71	53.29	$GdFeO_3$
d	480	SQ3	48.85	51.15	$GdFeO_3$

Based on X-ray and SEM/EDX data (Fig. 1(2,3), Table 1), samples treated at 300 ° C and 400 ° C under 70 MPa pressure for 1 hour contain $Gd(OH)_3$, FeOOH and small amounts of $Gd_3Fe_5O_{12}$ and $GdFeO_3$. At the same time, the presence of Gd_2O_3 and Fe_2O_3 are observed

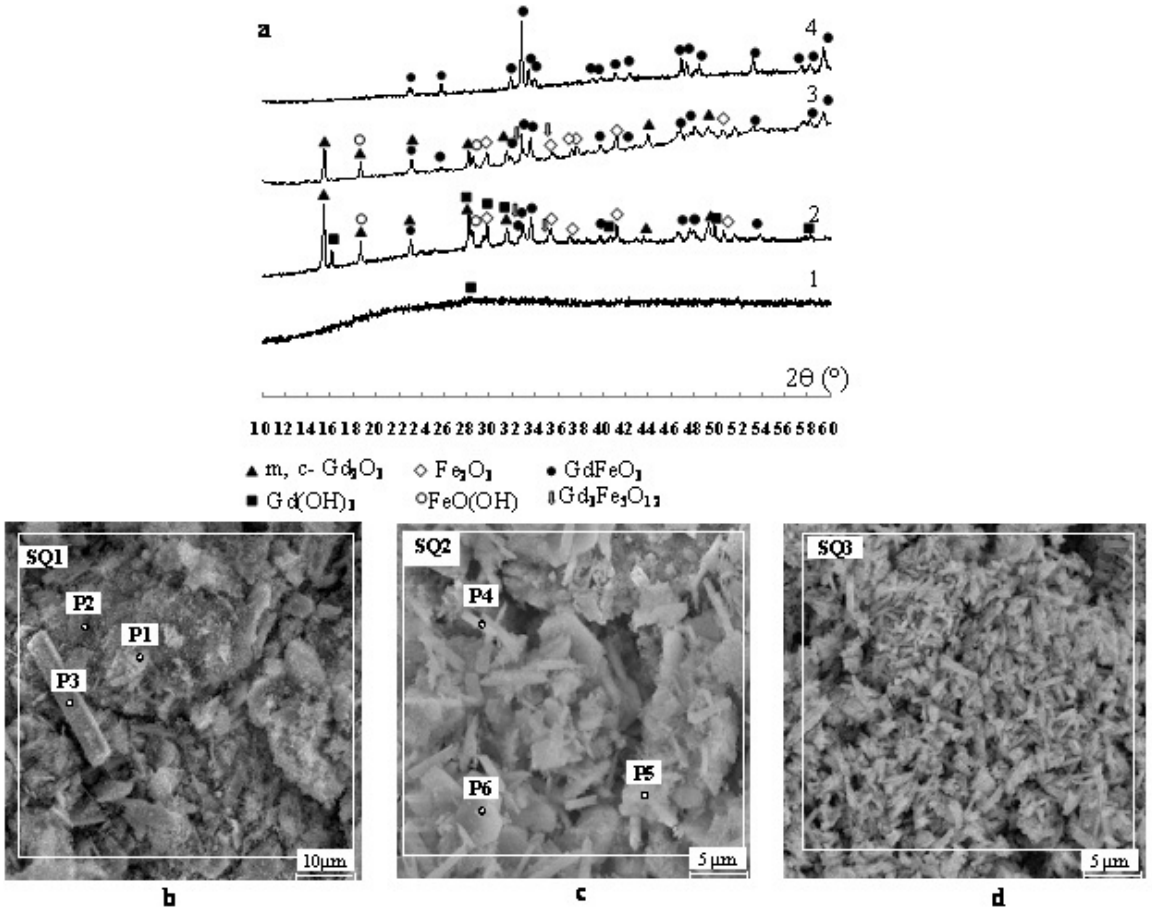

FIG. 1. **a)** X-Ray diffraction patterns and **b-d)** SEM photographs of: **1)** initial mixture, **2-4)**, **b-d)** initial mixtures after hydrothermal treatment at 300, 400, 480 ° C under 70 MPa for 1 h

TABLE 2. Electron probe microanalysis data for the regions indicated in Fig. 2(*b*,*c*)

Sample	Hydrothermal conditions	Examined region	Components content, mol%		Phases
			$GdO_{1.5}$	$FeO_{1.5}$	
b	600	SQ	46.71	53.29	$GdFeO_3$
		SQ1	46.79	53.21	
		1	47.64	52.36	
c	900	SQ	48.18	51.82	
		1	41.60	58.40	
		2	41.08	58.92	
		3	48.58	51.42	
		4	45.76	54.24	
		5	47.63	52.37	

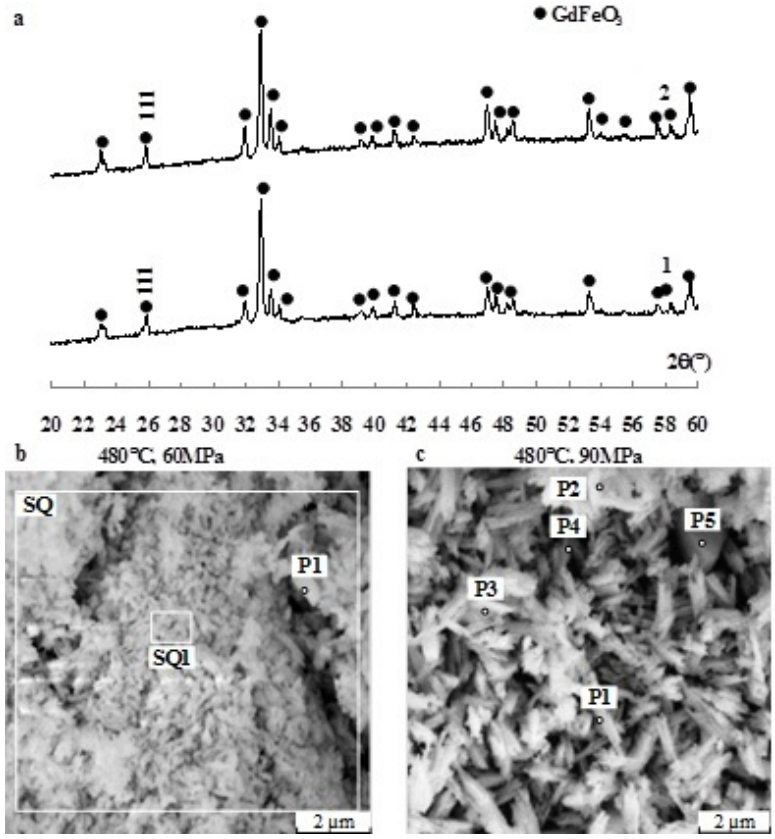

FIG. 2. **a)** X-Ray diffraction patterns and **b,c)** SEM photographs of initial mixtures after hydrothermal treatment at 480 °C under 60 MPa (1,b) and 90 MPa (2,c) for 1 h

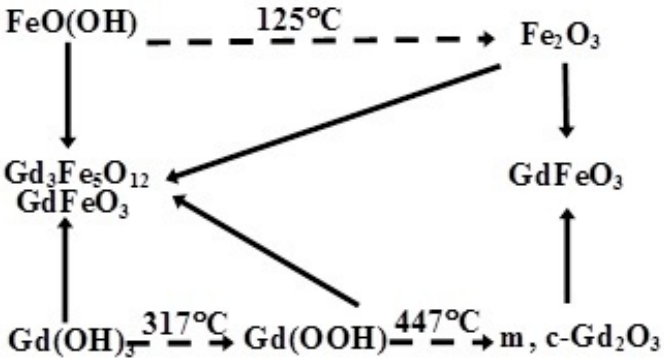

FIG. 3. Phase formation scheme, describing processes which are taken place under initial mixture hydrothermal treatment to yield $GdFeO_3$

(Fig. 1(2,3); Table 1). Raising the temperature rising to 480 ° C leads to homogeneous $GdFeO_3$ formation (Fig. 1(4), Table 1).

The formation of $GdFeO_3$ nanoparticles was investigated by varying pressure from 60 to 90 MPa and was carried out at the same temperature, 480 ° C. Fig. 2 and Table 2 present results for X-ray and SEM/EDX data of the initial mixture samples treated under 60 and 90 MPa at 480 ° C for 1 hour. According to the presented data (Fig. 2,*a* and Table 2), all characteristic reflects corresponded to the target product. The mean size of coherent scattering regions (D_{111}) was determined from X-ray data for peak with (111) index for samples of $GdFeO_3$ produced after initial mixture treatment under 60, 70, 90 MPa at 480 ° C. The D_{111} values were equal to 53, 68 and 73 nm, respectively. Figure 2(*b*,*c*) shows that the product was entirely composed of crystals with a relatively uniform, rod-like morphology.

Thus, according to presented and literature data [17, 18], the formation mechanism for $GdFeO_3$ nanoparticles under the hydrothermal conditions can be illustrated as the shown scheme (Fig. 3).

The large values of mean size of coherent scattering regions of $GdFeO_3$ nanoparticles can be explained by oriented attachment of nanocrystals proceeding via the described mechanism [19, 20].

4. Conclusion

These results showed that the mechanism by which $GdFeO_3$ nanoparticles were formed proceeded through the dehydration stages of $Gd(OH)_3$ and FeOOH. The target product was entirely composed of crystals with a relatively uniform, rod-like morphology. The large values of mean size of coherent scattering regions of $GdFeO_3$ nanoparticles ranging from 53–73 nm size were obviously attributed to oriented attachment of nanocrystals.

Acknowledgments

The authors would like to thank Prof. V. V. Gusarov for useful discussions.

This work was financially supported by the Russian Foundation for Basic Research, project N 13-03-12470 ofi_m2.

References

[1] I.A. Leonidov, M.V. Patrakeev , J.A. Bahteeva, K.V. Poholok, D.S. Filimonov, K.R. Poeppelmeier, V.L. Kozhevnikov. Oxygen-ion and electron conductivity in $Sr_2(Fe_{1-x}Ga_x)_2O_5$. *Journal of Solid State Chemistry*, **179**, P. 3045–3051 (2006).

[2] A.G. Petrosyan, V.F. Popova, V.L. Ugolkov, D.P. Romanov, K.L. Ovanesyan. A study of phase stability in the Lu_2O_3–Al_2O_3 system. *Journal of Crystal Growth*, **377**, P. 178–183 (2013).

[3] J.F. Scott. Magnetic phases of bismuth ferrite. *Journal of Magnetism and Magnetic Materials*, **321**, P. 1689–1691 (2009).

[4] T. Goto, T. Kimura, G. Lawes, A.P. Ramirez, Y. Tokura. Ferroelectricity and giant magnetocapacitance in perovskite rare-earth manganites. *Physical review letters*, **92**, P. 257201 (2004).

[5] T.I. Chupakhina, G.V. Bazuev. Synthesis, structure, and magnetic properties of $Sr_{0.8}Ce_{0.2}Mn_{1-y}Co_yO_{3-\delta}$ (y = 0.3, 0.4). *Inorganic Materials*, **47**(12), P. 1361–1366 (2011).

[6] J. Á Prado-Gonjal, M. Arévalo-López, E. Morán. Microwave-assisted synthesis: A fast and efficient route to produce $LaMO_3$ (M = Al, Cr, Mn, Fe, Co) perovskite materials. *Materials Research Bulletin*, **46**, P. 222–230 (2011).

[7] H. Shen, J. Xu, A. Wu. Preparation and characterization of perovskite $REFeO_3$ nanocrystalline powders. *Journal of Rare earths*, **28**(3), P.416–419 (2010).

[8] S. Goswami, D. Bhattacharya, P. Choudhury. Particle size dependence of magnetization and noncentrosymmetry in nanoscale $BiFeO_3$. *Journal of applied physics D*, **109**(7), P. 737–739 (2011).

[9] M. Sivakumar, A. Gedanken, D. Bhattacharya, I. Brukental, Y. Yeshurun, W. Zhong, Y.W. Du, I. Felner, I. Nowik. Sonochemical synthesis of nanocrystalline rare earth orthoferrites using $Fe(CO)_5$ precursor. *Chem. Mater*, **16**, P. 3623–3632 (2004).

[10] S. Nakayama. $LaFeO_3$ perovskite-type oxide prepared by oxide-mixing, co-precipitation and complex synthesis methods. *Journal of Materials Science*, **36**, P. 5643–5648 (2001).

[11] A.T. Nguyen, O.V. Almjasheva, I.Ya. Mittova, O.V. Stognei, S.A. Soldatenko. Synthesis and magnetic properties of $YFeO_3$ nanocrystals. *Inorganic Materials*, **45**(11), P. 1304–1308 (2009).

[12] I.Ya. Mittova, A.T. Nguyen, O.V. Almjasheva. Influence of the synthesis conditions on the particle size and morphology of yttrium orthoferrite obtained from aqueous solutions. *Russian Journal of Applied Chemistry*, **82**(11), P. 1915–1918 (2009).

[13] R. Lu, J. Yuan, H. Shi, Bin Li, W. Wang, D. Wang, M. Cao. Morphology-controlled synthesis and growth mechanism of lead-free bismuth sodium titanate nanostructures via the hydrothermal route. *CrystEngComm*, **15**, P. 3984–3991 (2013).

[14] M.V. Tomkovich, E.R. Andrievskaya, V.V. Gusarov. Formation under hydrothermal conditions and structural features of nanoparticles based on the system ZrO_2–Gd_2O_3. *Nanosystems: physics, chemistry, mathematics*, **2**(2), P. 6–14 (2011).

[15] E.A. Tugova, V.V. Gusarov. Structure peculiarities of nanocrystalline solid solutions in $GdAlO_3$ – $GdFeO_3$ system. *Nanosystems: physics, chemistry, mathematics*, **4**(3), P. 352–356 (2013).

[16] G.C. Kennedy. Pressure-volume-temperature relations in water at elevated temperatures and pressures. *American Journal of Science*, **248**, P. 540-564 (1950).

[17] M.W. Shafer, R. Roy. Rare-earth polymorphism and phase equilibria in rare-earth oxide-water systems. *Journal of the American Ceramic Society*, **42**(4), P. 563–570 (1959).

[18] Ch. Chang , Zhang Q.-an, Ma D. The hydrothermal preparation, crystal structure and photoluminescent properties of GdOOH nanorods. *Nanotechnology*, **17**, P. 1981–1985 (2006).

[19] R.L. Penn, J.F. Banfield. Imperfect oriented attachment: dislocation generation in defect-free nanocrystals. *Science* ,**281**, P. 969–971 (1998).

[20] R.L. Penn, J.F. Banfield. Oriented attachment and growth, twinning, polytypism, and formation of metastable phases: Insights from nanocrystalline TiO_2. *American Mineralogist*, **83**, P. 1077–1082 (1998).